Confined quantum systems: spectra of weakly bound electrons in a strongly anisotropic oblate harmonic oscillator potential

2005 J. Phys.: Condens. Matter 17 5159

(http://iopscience.iop.org/0953-8984/17/34/001)

INSTITUTE OF PHYSICS PUBLISHING JOURNAL OF PHYSICS: CONDENSED MATTER

J. Phys.: Condens. Matter **17** (2005) 5159–5178 doi:10.1088/0953-8984/17/34/001

Confined quantum systems: spectra of weakly bound electrons in a strongly anisotropic oblate harmonic oscillator potential

Tokuei Sako[1] **and Geerd H F Diercksen**[2]

[1] Laboratory of Physics, College of Science and Technology, Nihon University, 7-24-1 Narashinodai, Funabashi, 274-8501 Chiba, Japan
[2] Max-Planck-Institut für Astrophysik, Karl-Schwarzschild-Strasse 1, D-85741 Garching, Germany

Received 23 June 2005
Published 12 August 2005
Online at stacks.iop.org/JPhysCM/17/5159

Abstract

The spectrum and the electron density distribution of two, three, and four electrons confined by a strongly anisotropic oblate-type harmonic oscillator potential with small values of ω have been studied for all spin states by using the quantum chemical configuration interaction (CI) method employing large Cartesian anisotropic Gaussian basis sets. The convergence of the calculated energy spectrum with respect to different-size basis sets shows that an accuracy better than 2×10^{-6} has been obtained for the three-electron *harmonic oscillator quantum dot* by using a basis set including up to a k-type function, but that in order to achieve similar accuracy for the four-electron quantum dot the basis set has to be supplemented with functions as high as an m-type function. The analysis of the two leading configurations in the CI wavefunctions shows that large electron correlation prevails for the low lying states of the systems studied, particularly for the states with low spin multiplicity. Two types of electronic mode are identified, namely, the *circular mode* and the *breathing mode*. It is shown that the states having an excitation into the circular mode are energetically more favourable than those into the breathing mode when the strength of confinement ω is small.

1. Introduction

Semiconductor technology allows the construction of quantum systems consisting of electrons confined in potential wells, referred to as *artificial atoms* [1] or *quantum dots* [2, 3], as *double-dot artificial molecules* or *double quantum dots*, and as *quantum dot molecules* [4], respectively. Organic molecules in confined spaces have recently attracted the interest of many researchers in the field of chemical physics and physical chemistry. Studies on these *host–guest* systems

have been widely recognized as one of the most promising and rapidly emerging research areas in material and catalytic science [5].

The confinement has been modelled by an external one-particle potential introduced in an N-electron Schrödinger equation [6, 7]. Among the various forms of one-particle potentials introduced so far, harmonic oscillator potentials have been used most widely since, in addition to their simplicity, they can simulate the potential of quantum dots [2] as well as that of an atom or a molecule in a strong magnetic field [8, 9].

The Schrödinger equation for a single electron confined by a harmonic oscillator potential was solved in 1928 in closed form [10]. The solution of the Schrödinger equation becomes significantly more complicated for systems of two interacting electrons in a harmonic oscillator potential [11, 12], i.e. for two-electron *harmonic oscillator quantum dots* or *parabolic quantum dots*, because of the electron–electron interaction potential. Although in some cases analytical solutions are available also for confined two-electron systems [13], they are limited to the case of the spherical harmonic oscillator potential with specific values of ω. Therefore, the spectral properties of two-electron quantum dots, particularly those for *anisotropic* harmonic oscillator potentials [14–17], are still a subject of great interest.

Studies of multi-electron quantum dots require far more effort than those of one- and two-electron quantum dots. In this case the full configuration interaction (CI) method [18, 19] that can be used to study the spectral properties of two-electron systems is in general computationally not feasible since the dimension of the full CI matrix becomes extraordinary large when the number of interacting electrons exceeds two. Most previous studies on multi-electron quantum dots were based on either Hartree–Fock calculations [20–22] neglecting electron correlation completely, or on very limited CI calculations taking into account only a small part of the electron correlation. On the other hand, it has been recognized that electron correlation becomes increasingly important when the strength of the confinement becomes small [23–26]. Therefore, in order to study the energy spectra of multi-electron quantum dots with small values of ω it is necessary to introduce an efficient computational method that can be applied to systems with more than two electrons and accounts for electron correlation properly.

In the present study the spectral properties of multi-electron ($N = 2$, 3, and 4) harmonic oscillator quantum dots have been studied for all spin states by using a quantum chemical multi-reference configuration interaction method [27, 28] permitting us to reduce the size of the CI matrix significantly while keeping the accuracy sufficiently high. Large Cartesian anisotropic Gaussian basis sets have been developed in order to reproduce with high numerical accuracy the degeneracies in the energy spectra that originate from the analytical nature of the harmonic oscillator quantum dots [29, 30]. The computed spectra have been examined with respect to the variation of ω. Atomic units are used throughout this paper.

2. Computational methodology

2.1. Schrödinger equation

The Schrödinger equation for N-electrons confined by a potential $\mathcal{W}$ is given by (in atomic units)

$$[\mathcal{H}(\boldsymbol{r}) + \mathcal{W}(\boldsymbol{r})]\,\Psi(1, 2, \ldots, N) = E\Psi(1, 2, \ldots, N), \tag{1}$$

where the set $(1, 2, \ldots, N)$ denotes the orbital and the spin coordinates of the electrons. The operator $\mathcal{H}$ represents the N-electron operators describing the kinetic energy and the electron

interaction potentials:

$$\mathcal{H}(\boldsymbol{r}) = \sum_{i=1}^{N}\left[-\frac{1}{2}\nabla_i^2\right] + \sum_{i>j}^{N}\left[\frac{1}{|\mathbf{r}_i - \mathbf{r}_j|}\right], \tag{2}$$

where $\boldsymbol{r} \equiv \{\boldsymbol{r}_1, \boldsymbol{r}_2, \ldots, \boldsymbol{r}_N\}$ stands for the spatial coordinates of the electrons. The N-electron interaction potential is defined as the sum of one-electron contributions:

$$\mathcal{W}(\boldsymbol{r}) = \sum_{i=1}^{N} w(\boldsymbol{r}_i). \tag{3}$$

The one-particle confining potential $w(\boldsymbol{r}_i)$ is chosen to be an *anisotropic* harmonic oscillator potential:

$$w(\boldsymbol{r}_i) = \tfrac{1}{2}\left[\omega_x^2 x_i^2 + \omega_y^2 y_i^2 + \omega_z^2 z_i^2\right], \tag{4}$$

where $\boldsymbol{r}_i = \{x_i, y_i, z_i\}$. It is known that the potential of equation (4) is suitable for modelling the confining potential of semiconductor quantum dots [2].

The total energies of the confined quantum system have been calculated as the eigenvalues of the CI matrix. A full CI wavefunction has been used in the case of two-electron quantum dots while a multi-reference (MR) CI wavefunction has been used in the case of three- and four-electron quantum dots. All calculations have been performed by using OpenMol [31], an object-oriented program that originated in the Molecular Physics Group of the Max Planck Institute for Astrophysics and is being developed in international cooperation amongst individual researchers primarily for their own use. For the study of confined quantum systems, OpenMol has been extended to account for power series potentials and *anisotropic* Gaussian basis functions. The electron density plots have been generated by using the gOpenMol program [32].

2.2. Basis set

In a previous study of this series [16] *anisotropic* Gaussian-type orbitals (aniGTOs) have been introduced to correctly approximate the wavefunction of electrons confined in an anisotropic harmonic oscillator potential. Anisotropic Gaussian basis sets have been used also in studies of atoms in strong magnetic fields [8, 9] and of semiconductor quantum dots [18, 33]. A basis set of Cartesian anisotropic Gaussian-type orbitals (c-aniGTO) including one function for each type of orbital has the following general form:

$$\chi^{c}_{\vec{a},\vec{\zeta}}(\vec{r}) = x^{a_x} y^{a_y} z^{a_z} \exp(-\zeta_x x^2 - \zeta_y y^2 - \zeta_z z^2). \tag{5}$$

The orbital exponents are chosen to be $(\zeta_x, \zeta_y, \zeta_z) = (\omega_x/2, \omega_y/2, \omega_z/2)$. Following the quantum chemical convention, these orbitals are classified as s-, p-, d-type, $\cdots$ for $a = a_x + a_y + a_z = 0, 1, 2, \ldots$, respectively.

In order to check the reliability of c-aniGTO basis sets for calculating the energy spectra of strongly anisotropic harmonic oscillator quantum dots the energies of the six lowest doublet states of three electrons confined by an anisotropic harmonic oscillator potential with $(\omega_x, \omega_y, \omega_z) = (0.01, 0.01, 0.1)$ have been calculated for different-size basis sets. The resulting energy spectra are displayed in figure 1 for five different c-aniGTO basis sets. All basis sets consist of one function for each type of orbital. The smallest *normal* basis of 56 functions consists of functions from s- to h-type, described by [1s1p1d1f1g1h]. The term *normal* applies to the c-aniGTO basis sets that include all angular functions defined by equation (5), while a *reduced* c-aniGTO basis set, which will be introduced later, is a subset of a normal c-aniGTO basis set. The next larger normal c-aniGTO basis set of 84 functions consists of functions up

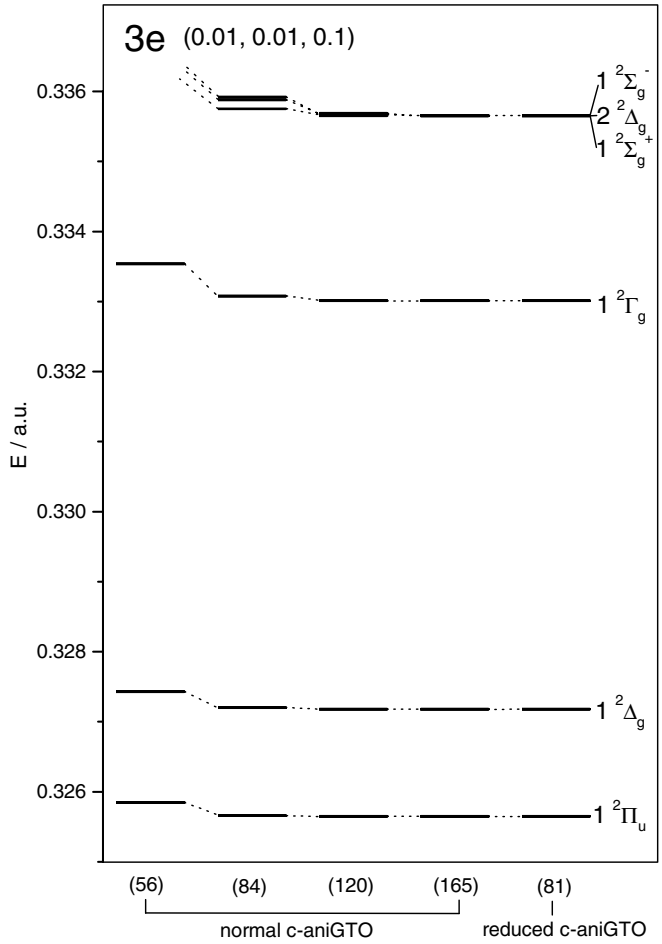

Figure 1. Spectra of the low lying doublet states of three electrons confined by an oblate-type harmonic oscillator potential with $(\omega_x, \omega_y, \omega_z) = (0.01, 0.01, 0.1)$ for different Cartesian anisotropic Gaussian basis sets. The numbers in the round brackets represent the total numbers of basis functions.

to i-type. The normal basis sets of 120 and of 165 functions consist of functions up to j-type and k-type functions, respectively.

As shown in figure 1 the energy spectra converge with increasing size of the normal c-aniGTO basis sets. The energy levels calculated using the smallest basis set are displayed at the far left-hand side of figure 1. They are shifted strongly toward the higher energies indicating that the smallest basis set of 56 functions is not sufficiently large for calculating the energy spectra. The CI energies of the lowest $1\,^2\Pi_u$ state and of the first excited $1\,^2\Delta_g$ state calculated by using the next larger basis set of 84 functions agree with those calculated by using the larger basis sets within 2×10^{-5}, but the agreement becomes significantly worse for the higher lying states.

It is noted that the basis set of 84 functions including up to i-type functions, described by [1s1p1d1f1g1h1i], has been explored in previous studies of anisotropic harmonic oscillator quantum dots and proved in that case to be sufficient for calculating reliable low lying energy spectra [16, 29, 30]. The present results show that the calculation of reliable energy spectra of

strongly anisotropic quantum dots requires even higher angular momentum functions in the basis set. The energies of all states displayed in figure 1 agree with each other within 4×10^{-5} for the two larger basis sets, that is for the basis sets of 120 functions and of 165 functions. It is noted, however, that the highest three states $1\ ^2\Sigma_g^+$, $2\ ^2\Delta_g$, and $1\ ^2\Sigma_g^-$ are split slightly for the basis set of 120 functions while they are degenerate for the larger basis set of 165 functions within 2×10^{-6}. As will be discussed in a later section, these three states should indeed be degenerate owing to an analytical property of harmonic oscillator quantum dots [30].

The energy spectrum displayed at the far right-hand side of figure 1, calculated by using the *reduced* c-aniGTO basis set of 81 functions, agrees with that calculated by using the largest *normal* basis set of 165 functions within 2×10^{-6}. This reduced c-aniGTO basis set is obtained from the largest normal c-aniGTO basis set of 165 functions by deleting all functions with a_z larger than one, that is by deleting all functions with more than one node along the z axis. Since for the confinement potential in the present case ω_z is ten times larger than ω_x and ω_y, the orbitals with nodes along the z axis have much larger orbital energies than those without nodes along the z axis and consequently do not contribute to the energies of the low lying states. This reduced basis set is further extended up to l-type functions and the resulting reduced c-aniGTO basis set of 100 functions, described by [1s1p1d1f1g1h1i1j1k1l], is used for the rest of the calculations in this study.

The CI matrix is constructed by using symmetry-adapted configuration state functions (CFS) and is block diagonal with respect to a given spin configuration and a given symmetry species in D_{2h}. The one-particle orbitals used to construct the CSFs are obtained by solving the closed-shell Hartree–Fock–Roothaan equations for the two-electron quantum dot. The typical dimension of a block in the CI matrix is between 600 and 700 for the two-electron quantum dots, between 15 000 and 30 000 for the three-electron quantum dot, and between 100 000 and 200 000 for the four-electron quantum dot.

3. Results and discussion

3.1. Energy spectra and electron density distributions

3.1.1. Hartree–Fock orbitals. The closed-shell Hartree–Fock orbital energies and density distributions for two electrons confined by an anisotropic harmonic oscillator potential with $(\omega_x, \omega_y, \omega_z) = (0.01, 0.01, 0.1)$ have been calculated and are displayed in figure 2. The density distribution is displayed in cubes with a side length of 48 au. The z axis is directed along the vertical edge of the cube. The density at the surface is 5.0×10^{-5}. The orbitals have been assigned by using the notation $[v_x + v_y, v_z]\Delta$, defined in a previous study [16], where v_x, v_y, and v_z denote one-electron harmonic oscillator quantum numbers for the x, y, and z coordinates, respectively, and Δ denotes the symmetry labels of the $D_{\infty,h}$ group. Owing to the axial symmetry of the confining potential the z component of the angular momentum quantum number, l_z, is conserved. It is related to the v_z and v_y quantum numbers by $l_z = v_x - v_y$ [34].

The low lying orbitals displayed in figure 2 do not have a nodal plane along the z axis. Their v_z quantum number is zero. This is consistent with the result of the previous section demonstrating that the energy spectrum calculated using the *reduced* c-aniGTO basis set of 81 functions is almost identical for the low lying states to that calculated using the corresponding normal c-aniGTO basis set of 165 functions. It is interesting to compare the energy level sequence of the *one-electron* harmonic oscillator quantum dot to the Hartree–Fock orbital energy sequence displayed in figure 2 for the same confining potential. In the case of the one-electron quantum dot a set of levels belonging to the same $[v_x + v_y, v_z]$ manifold have the same energy. For example, the two levels $[2, 0]\delta_g$ and $[2, 0]\sigma_g$ in the $[2, 0]$ manifold, the two levels $[3, 0]\phi_u$ and $[3, 0]\pi_u$ in the $[3, 0]$ manifold, and the three levels $[4, 0]\gamma_g$, $[4, 0]\delta_g$,

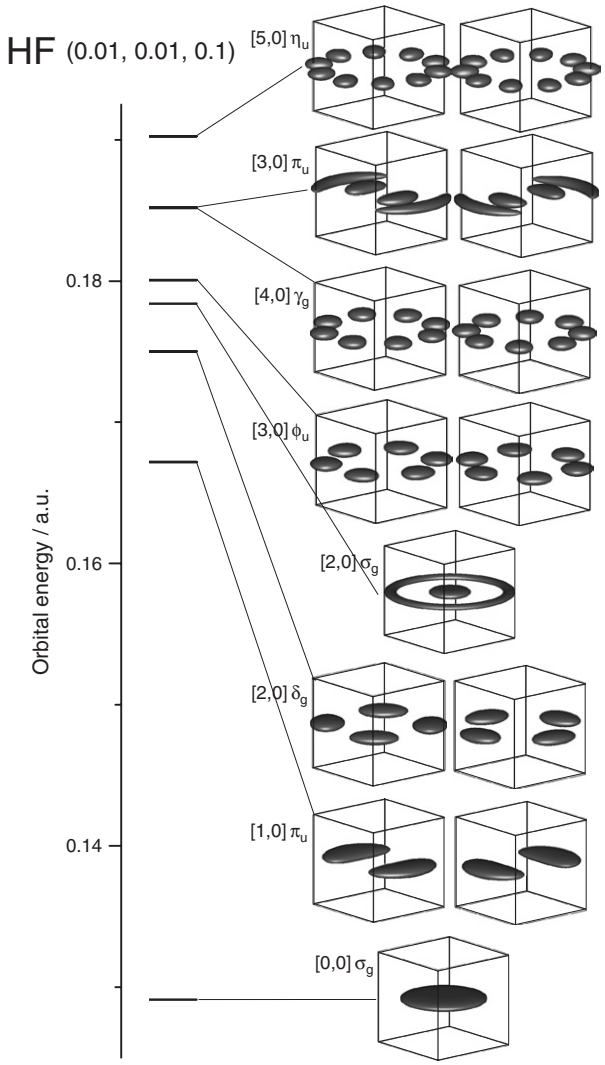

Figure 2. The closed-shell Hartree–Fock orbital density distribution for two electrons confined by an oblate-type harmonic oscillator potential with $(\omega_x, \omega_y, \omega_z) = (0.01, 0.01, 0.1)$. The density at the surface is 5.0×10^{-5}.

and $[4, 0]\sigma_g$ in the [4, 0] manifold, etc, are degenerate within their respective manifolds. On the other hand, in the case of the Hartree–Fock orbitals the set of levels belonging to the same $[v_x + v_y, v_z]$ manifold are not degenerate but are split as shown in figure 2. This is attributed to a large contribution to the energy from the electron–electron interaction which strongly changes the shell structure determined by the harmonic oscillator potential.

Two types of *electron mode* can be identified from the nodal patterns of the Hartree–Fock orbitals displayed in figure 2 representing the bound motion of electrons analogous to *vibrational modes* in molecular vibrational spectroscopy, namely: the *circular mode* with angular nodal planes dividing the orbitals through the centre parallel to the z axis, and the *breathing mode* with radial nodal planes dividing the orbitals with respect to the centre. The number of angular nodal planes specifies the orbital angular momentum and is equal to the $|l_z|$

Table 1. The CI energy (in au) of the six lowest singlet and triplet states of two electrons confined by an oblate-type harmonic oscillator potential with $(\omega_x, \omega_y, \omega_z) = (0.01, 0.01, 0.1)$.

Singlet		Triplet	
$1\,^1\Sigma_g^+$	0.173 506		
		$1\,^3\Pi_u$	0.174 987
$1\,^1\Delta_g$	0.178 953		
$1\,^1\Pi_u$	0.183 506		
		$1\,^3\Phi_u$	0.184 602
		$1\,^3\Sigma_g^-$	0.184 987
		$1\,^3\Delta_g$	0.184 987
		$1\,^3\Sigma_g^+$	0.184 987
$2\,^1\Pi_u$	0.188 953		
$1\,^1\Phi_u$	0.188 953		
$2\,^1\Sigma_g^+$	0.191 057		
		$2\,^3\Pi_u$	0.192 769

value while the number of radial nodal planes is equal to the $v_x + v_y - |l_z|$ value. The circular mode may be interpreted classically as corresponding to a circular motion of the electron around the symmetry axis of the confining potential and the breathing mode as a radial motion of the electron.

It is noted that within each $[v_x + v_y, v_z]$ manifold, orbitals with larger $|l_z|$ quantum numbers have lower orbital energies. For example, within the [2, 0] manifold the δ_g orbital has a lower energy than the σ_g orbital and within the [3, 0] manifold the ϕ_u orbital has a lower energy than the π_u orbital and so on. This trend of the Hartree–Fock orbital energy sequence indicates that the circular mode is energetically preferable to the breathing mode.

3.1.2. The two-electron quantum dot. The energy spectra and the electron density distributions of the six lowest singlet states and of the six lowest triplet states of two electrons confined by an oblate-type harmonic oscillator potential with $(\omega_x, \omega_y, \omega_z) = (0.01, 0.01, 0.10)$ are displayed in figures 3 and 4, respectively. The CI energies are listed in table 1 in increasing order. The electron density distributions are displayed in the same way as for the Hartree–Fock orbitals except that the density at the surface is 1.0×10^{-4}. The lowest state in the singlet manifold is $1\,^1\Sigma_g^+$ as expected from the Hartree–Fock orbitals displayed in figure 2. However, the first and the second excited states in the singlet manifold are $1\,^1\Delta_g$ and $1\,^1\Pi_u$, respectively. This order differs from that of the Hartree–Fock orbital sequence. A reversed order of states as compared to the Hartree–Fock orbital sequence is observed also in the triplet manifold. The lowest triplet state is $1\,^3\Pi_u$ as expected, but the first excited state is not $1\,^3\Delta_g$ but $1\,^3\Phi_u$. The reversed order of states as compared to the one-electron Hartree–Fock orbital sequence indicates that even the lowest excited states cannot be described by a simple one-electron excitation from the ground state configuration, as is possible for conventional two-electron atoms like He.

Another interesting observation concerns the degeneracy of states. From figures 3 and 4 it is evident that the two states $2\,^1\Pi_u$ and $1\,^1\Phi_u$ in the singlet manifold, and the three states $1\,^3\Sigma_g^+$, $1\,^3\Sigma_g^-$ and $1\,^3\Delta_g$ in the triplet manifold are degenerate. This degeneracy is not accidental but a direct consequence of the analytical properties of harmonic oscillator quantum dots. As known from the generalization of *Kohn's theorem* [35–38] the excitation energy in dipole-allowed transitions is identical to the fundamental frequency of the harmonic oscillator confining potential. In the present case transitions to the $2\,^1\Pi_u$ and the $1\,^1\Phi_u$ state are dipole

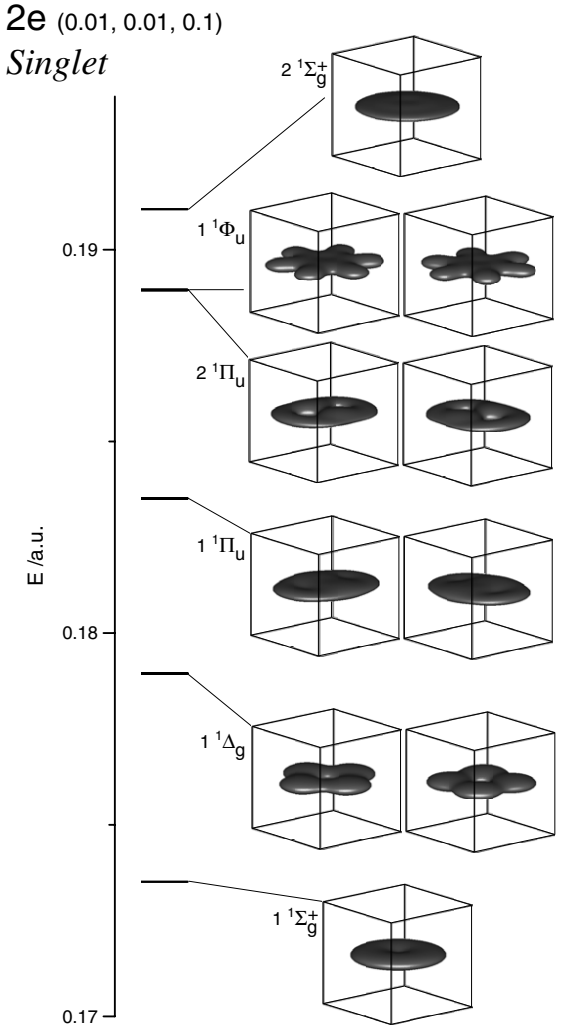

Figure 3. The CI energy and electron density distribution of the six lowest singlet states of two electrons confined by an oblate-type harmonic oscillator potential with $(\omega_x, \omega_y, \omega_z) = (0.01, 0.01, 0.1)$. The density at the surface is 1.0×10^{-4}.

allowed from the $1\ ^1\Delta_g$ state, and transitions to the $1\ ^3\Sigma_g^+$, the $1\ ^3\Sigma_g^-$ and the $1\ ^3\Delta_g$ state are the dipole allowed from the $1\ ^3\Pi_u$ state.

The CI energies listed in table 1 confirm these results. The CI energies of the $2\ ^1\Pi_u$ and the $1\ ^1\Phi_u$ states are identical within 1.0×10^{-6} and the energy of excitation to these states from the $1\ ^1\Delta_g$ state is equal to the smaller of the harmonic frequencies, ω_x $(=\omega_y)$, of 0.01 within 1.0×10^{-6}. The situation is similar for the triplet manifold. The CI energies of the three states $1\ ^3\Sigma_g^+$, $1\ ^3\Sigma_g^-$, and $1\ ^3\Delta_g$ are identical and the energy of excitation to these states from the $1\ ^3\Pi_u$ state is equal to 0.01 within 1.0×10^{-6}. It can be seen from table 1 that the energy of excitation to the $1\ ^1\Pi_u$ state from the $1\ ^1\Sigma_g^+$ state is also equal to 0.01. All these transitions are dipole allowed. It is noted that the correct degeneracy and the accuracy of the excitation energies are strongly dependent on the quality of the basis set. This means in turn that these properties can be used to check the quality of the calculations.

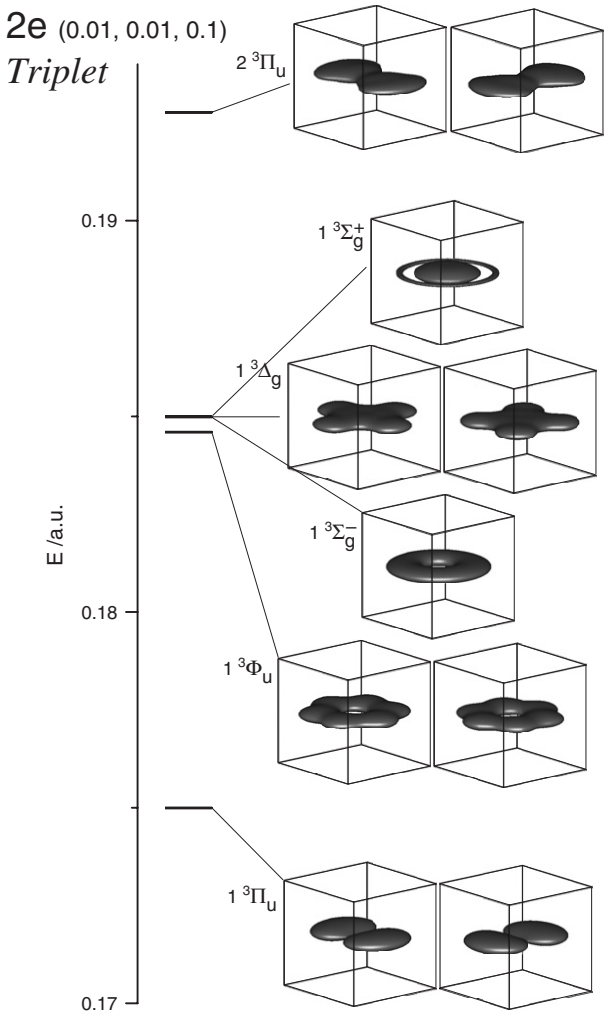

Figure 4. The CI energy and electron density distribution of the six lowest triplet states of two electrons confined by an oblate-type harmonic oscillator potential with $(\omega_x, \omega_y, \omega_z) = (0.01, 0.01, 0.1)$. The density at the surface is 1.0×10^{-4}.

The two leading configurations and their contributions to the CI wavefunction are listed in tables 2 and 3 for the six lowest singlet and the six lowest triplet states, respectively. The leading configuration of the $1\ ^1\Sigma_g^+$ ground state is the Hartree–Fock ground state $([0, 0]\sigma_g)^2$ as expected from the Hartree–Fock orbital diagram displayed in figure 2. But even for this Hartree–Fock ground state the square norm is only 0.582. That means it contributes less than 60% to the $1\ ^1\Sigma_g^+$ state. This indicates a large electron correlation effect in harmonic oscillator quantum dots [16]. The leading configuration of the first excited $1\ ^1\Delta_g$ state is $([0, 0]\sigma_g)([2, 0]\delta_g)$, a single excitation from the ground state configuration $([0, 0]\sigma_g)^2$ with a square norm as small as 0.276. On the other hand, the second-leading configuration $([1, 0]\pi_u)^2$ is a double excitation from the ground state and makes a contribution to the $1\ ^1\Delta_g$ state similar to the first-leading configuration. This indicates that multiple excitations play important roles for these low lying states.

Table 2. The two leading configurations and their squared norms for the six lowest singlet states of two electrons confined by an oblate-type harmonic oscillator potential with $(\omega_x, \omega_y, \omega_z) = (0.01, 0.01, 0.1)$.

State	Config. 1	Norm 1	Config. 2	Norm 2
$1\,^1\Sigma_g^+$	$([0,0]\sigma_g)^2$	0.582	$([1,0]\pi_u)^2$	0.153
$1\,^1\Delta_g$	$([0,0]\sigma_g)([2,0]\delta_g)$	0.276	$([1,0]\pi_u)^2$	0.230
$1\,^1\Pi_u$	$([0,0]\sigma_g)([1,0]\pi_u)$	0.415	$([1,0]\pi_u)([2,0]\delta_g)$	0.126
$2\,^1\Pi_u$	$([1,0]\pi_u)([2,0]\sigma_g)$	0.174	$([0,0]\sigma_g)([3,0]\pi_u)$	0.135
$1\,^1\Phi_u$	$([0,0]\sigma_g)([3,0]\phi_u)$	0.395	$([0,0]\sigma_g)([5,0]\phi_u)$	0.172
$2\,^1\Sigma_g^+$	$([0,0]\sigma_g)([2,0]\sigma_g)$	0.305	$([1,0]\pi_u)^2$	0.229

Table 3. The two leading configurations and their squared norms for the six lowest triplet states of two electrons confined by an oblate-type harmonic oscillator potential with $(\omega_x, \omega_y, \omega_z) = (0.01, 0.01, 0.1)$.

State	Config. 1	Norm 1	Config. 2	Norm 2
$1\,^3\Pi_u$	$([0,0]\sigma_g)([1,0]\pi_u)$	0.621	$([0,0]\sigma_g)([3,0]\pi_u)$	0.171
$1\,^3\Phi_u$	$([1,0]\pi_u)([2,0]\delta_g)$	0.282	$([1,0]\pi_u)([4,0]\delta_g)$	0.170
$1\,^3\Sigma_g^-$	$([1,0]\pi_u)([1,0]\pi_u)$	0.430	$([1,0]\pi_u)([3,0]\pi_u)$	0.238
$1\,^3\Delta_g$	$([0,0]\sigma_g)([2,0]\delta_g)$	0.505	$([0,0]\sigma_g)([4,0]\delta_g)$	0.152
$1\,^3\Sigma_g^+$	$([0,0]\sigma_g)([2,0]\sigma_g)$	0.463	$([0,0]\sigma_g)([4,0]\sigma_g)$	0.285
$2\,^3\Pi_u$	$([1,0]\pi_u)([2,0]\sigma_g)$	0.161	$([1,0]\pi_u)([2,0]\delta_g)$	0.146

In the case of the triplet manifold the leading configuration of the lowest $1\,^3\Pi_u$ state is $([0,0]\sigma_g)([1,0]\pi_u)$ as expected from the Hartree–Fock orbital diagram displayed in figure 2. It is noted that in this case the square norm of the leading configuration of 0.621 is larger than that of the leading Hartree–Fock ground state configuration $([0,0]\sigma_g)^2$ in the $1\,^1\Sigma_g^+$ ground state of 0.582. It is interesting to compare the contributions of the $([0,0]\sigma_g)([1,0]\pi_u)$ configuration to this triplet $1\,^3\Pi_u$ state and to the corresponding singlet $1\,^1\Pi_u$ state. Although the two states have the same primary configuration of $([0,0]\sigma_g)([1,0]\pi_u)$, the square norm of this contribution in the triplet state of 0.621 is much larger than that in the singlet state of 0.415. This indicates that the electron correlation is smaller in the triplet state than in the singlet state [39]. A similar trend can be observed in the $1\,^3\Sigma_g^+$ and $2\,^1\Sigma_g^+$ states. The leading configuration $([0,0]\sigma_g)([2,0]\sigma_g)$ has a contribution of 0.463 in the triplet state and 0.305 in the singlet state.

It is interesting to compare the electron density distribution of the *singlet–triplet* pairs of states. In the case of the $1\,^1\Pi_u$–$1\,^3\Pi_u$ pair the electron density distributions for both states, displayed in figures 3 and 4, have a twofold symmetry with respect to the z axis indicating π symmetry. On the other hand, the electron density distribution of the triplet $1\,^3\Pi_u$ state displayed in figure 4 has a node in the middle while that of the singlet $1\,^1\Pi_u$ state shown in figure 3 has no node on the surface. By referring to the shape of the Hartree–Fock orbitals displayed in figure 2, it can be seen that the node on the surface of the electron density distribution of the $1\,^3\Pi_u$ state originates from the node of the $[1,0]\pi_u$ orbital. This interpretation is consistent with the analysis of the CI wavefunctions. It shows that the $1\,^3\Pi_u$ state has a larger contribution from the $([0,0]\sigma_g)([1,0]\pi_u)$ configuration than from the $1\,^1\Pi_u$ state. The larger configuration mixing in the singlet state may in addition blur the nodal pattern. The situation is similar for the $1\,^3\Sigma_g^+$–$2\,^1\Sigma_g^+$ pair. The electron density distribution of the $2\,^1\Sigma_g^+$ state is a simple disc while that of the $1\,^3\Sigma_g^+$ has an outer ring that is characteristic of the nodal pattern in the $[2,0]\sigma_g$ orbital displayed in figure 2.

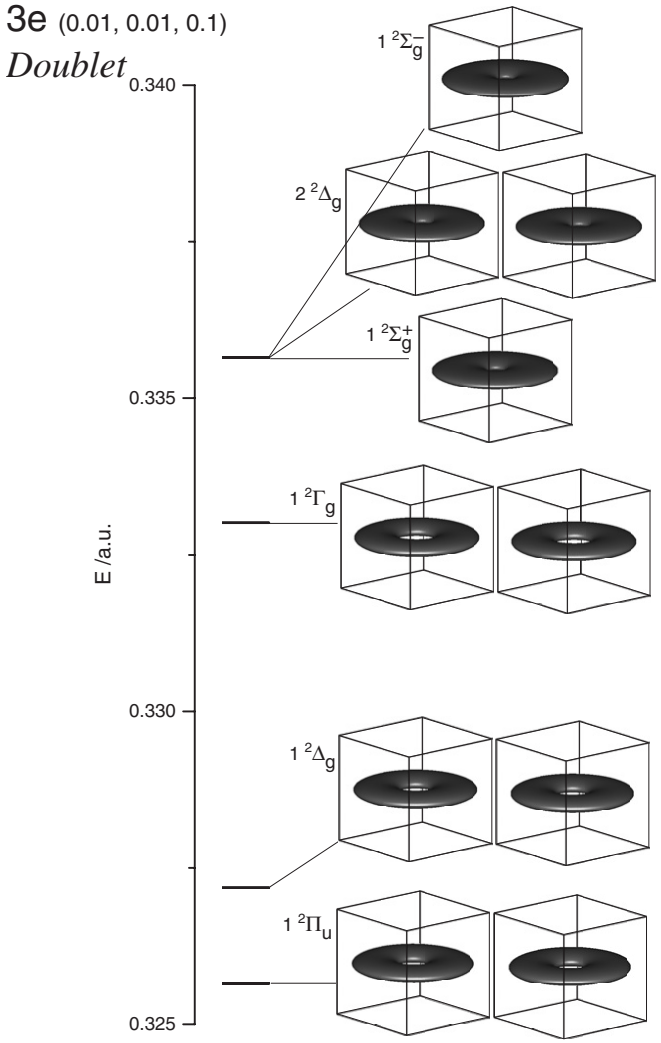

Figure 5. The CI energy and electron density distribution of the six lowest doublet states of three electrons confined by an oblate-type harmonic oscillator potential with $(\omega_x, \omega_y, \omega_z) = (0.01, 0.01, 0.1)$. The density at the surface is 1.0×10^{-4}.

3.1.3. The three-electron quantum dot. The energy spectra and the electron density distributions of the six lowest doublet states and of the six lowest quartet states of three electrons confined by an oblate-type harmonic oscillator potential with $(\omega_x, \omega_y, \omega_z) = (0.01, 0.01, 0.10)$ are displayed in figures 5 and 6, respectively. The CI energies are listed in table 4 in increasing order. The electron density distributions are displayed in the same way as for the two-electron quantum dots.

On inspection of the energies displayed in table 4, it is noted that the ground state of the three-electron quantum dot is not the *doublet* $1\ ^2\Pi_u$ state but the *quartet* $1\ ^4\Sigma_g^-$ state which is contrary to what is expected from the Hartree–Fock orbital sequence. This contradiction is a clear manifestation of the fact that the energy stabilization originating from the exchange interaction is large enough to excite one electron from the lowest $[0, 0]\sigma_g$ orbital to the next

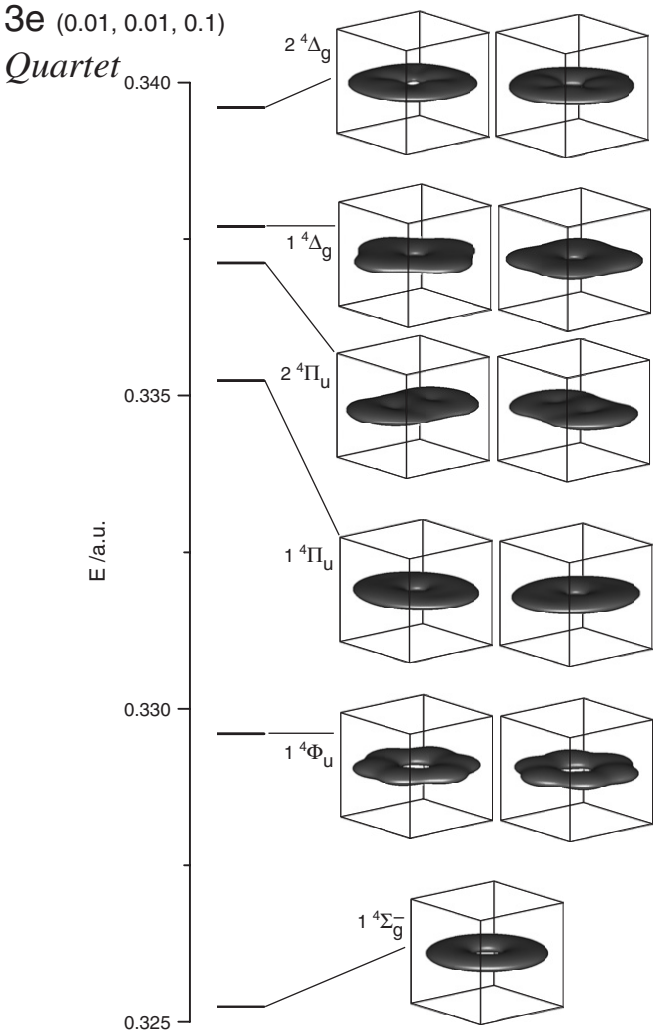

Figure 6. The CI energy and electron density distribution of the six lowest quartet states of three electrons confined by an oblate-type harmonic oscillator potential with $(\omega_x, \omega_y, \omega_z) = (0.01, 0.01, 0.1)$. The density at the surface is 1.0×10^{-4}.

higher $[1, 0]\pi_u$ orbital. When the energy gap between these two orbitals becomes large to the extent that the energy gap is larger than the stabilization energy, the doublet $1\,^2\Pi_u$ state becomes the ground state.

As demonstrated for the two-electron quantum dot, the dipole-allowed states can be easily identified from the CI energies listed in table 4. In the doublet manifold the energy of excitation from the lowest $1\,^2\Pi_u$ state to the triply degenerate states $1\,^2\Delta_g$, $1\,^2\Sigma_g^+$, and $1\,^2\Sigma_g^-$ is equal to the confinement strength, ω_x $(=\omega_y)$, of 0.01 within 1.0×10^{-6} indicating that the corresponding transitions are dipole allowed. In the quartet manifold the energy of excitation from the ground $1\,^4\Sigma_g^-$ state to the $1\,^4\pi_u$ state and the energy of excitation from the $1\,^4\Phi_u$ state to the $2\,^4\Delta_g$ state are equal to 0.01. This indicates again that the corresponding transitions are dipole allowed. It is noted that the unlisted seventh-lowest state in the quartet manifold, $1\,^4\Gamma_g$, forms a degenerate pair with the $2\,^4\Delta_g$ state with a dipole-allowed transition from the $1\,^1\Phi_u$.

Table 4. The CI energy (in au) of the six lowest doublet and quartet states of three electrons confined by an oblate-type harmonic oscillator potential with $(\omega_x, \omega_y, \omega_z) = (0.01, 0.01, 0.1)$.

Doublet		Quartet	
		$1\,^4\Sigma_g^-$	0.325 237
$1\,^2\Pi_u$	0.325 647		
$1\,^2\Delta_g$	0.327 178		
		$1\,^4\Phi_u$	0.329 597
$1\,^2\Gamma_g$	0.333 007		
		$1\,^4\Pi_u$	0.335 237
$1\,^2\Delta_g$	0.335 647		
$1\,^2\Sigma_g^+$	0.335 647		
$1\,^2\Sigma_g^-$	0.335 647		
		$2\,^4\Pi_u$	0.337 123
		$1\,^4\Delta_g$	0.337 699
		$2\,^4\Delta_g$	0.339 597

The leading and the second-leading configuration and their square norms in the CI wavefunctions are listed for the six lowest doublet and quartet states in tables 5 and 6, respectively. It can be seen from these tables that the norm of the first-leading configuration in the quartet manifold tends to be larger than in the doublet manifold, as has been observed for the low lying *singlet–triplet* pairs of states of the two-electron quantum dot. This result can be most clearly seen in the present case for the $1\,^2\Sigma_g^-$–$1\,^4\Sigma_g^-$ pair. The leading configuration $([0, 0]\sigma_g)([1, 0]\pi_u)([1, 0]\pi_u)$ makes a contribution of 0.246 in the $1\,^2\Sigma_g^-$ state but makes a contribution as large as 0.633 in the $1\,^4\Sigma_g^-$ state. This indicates that the electron correlation has a much smaller effect in the quartet state than in the doublet state.

The electron density distributions of the two states of this doublet–quartet pair displayed in figures 5 and 6 are distinctly different. The electron density distribution of the $1\,^4\Sigma_g^-$ state has the form of a *ring*, while that of the $1\,^2\Sigma_g^-$ state is a *disc* with a very small hole at the centre. As the electron density distributions are displayed as surfaces for a specific value of density, the absence of the surface in some region does not mean necessarily that the density in that region is exactly zero: it may have any value smaller than the value of the plotted electron density surface. The reason for the larger area of low density in the electron density distribution of the $1\,^4\Sigma_g^-$ state as compared to the $1\,^2\Sigma_g^-$ state may be rationalized by inspecting the leading configurations in the corresponding CI wavefunctions. As shown in tables 5 and 6, the $1\,^4\Sigma_g^-$ state is dominated by the $([0, 0]\sigma_g)([1, 0]\pi_u)([1, 0]\pi_u)$ configuration, while the $1\,^2\Sigma_g^-$ state has only a contribution of 25% from this configuration. Since the $[1, 0]\pi_u$ orbital has a node in the middle of the density distribution, the electron density distribution of the $1\,^4\Sigma_g^-$ state has a lower density in the central region. On the other hand, in the case of the $1\,^2\Sigma_g^-$ state a larger contribution from different configurations fills the central region.

3.1.4. The four-electron quantum dot. The energy spectra and the electron density distributions of the six lowest singlet states, the six lowest triplet states, and the six lowest quintet states of four electrons confined by an oblate-type harmonic oscillator potential with $(\omega_x, \omega_y, \omega_z) = (0.01, 0.01, 0.10)$ are displayed in figures 7, 8, and 9, respectively. The CI energies are listed in table 7 in increasing order. The electron density distributions are displayed in the same way as for the two- and three-electron quantum dots.

As shown in table 7, the electronic ground state is the *triplet* $1\,^3\Sigma_g^-$ state and the first excited state is the lowest *singlet* $1\,^1\Sigma_g^+$ state. The lowest *quintet* state is the fourth excited

Table 5. The two leading configurations and their squared norms for the six lowest doublet states of three electrons confined by an oblate-type harmonic oscillator potential with $(\omega_x, \omega_y, \omega_z) = (0.01, 0.01, 0.1)$.

State	Config. 1	Norm 1	Config. 2	Norm 2
$1\,^2\Pi_u$	$([0,0]\sigma_g)^2([1,0]\pi_u)$	0.331	$([0,0]\sigma_g)([1,0]\pi_u)([2,0]\delta_g)$	0.159
$1\,^2\Delta_g$	$([0,0]\sigma_g)([1,0]\pi_u)([1,0]\pi_u)$	0.297	$([0,0]\sigma_g)^2([2,0]\delta_g)$	0.167
$1\,^2\Gamma_g$	$([0,0]\sigma_g)([1,0]\pi_u)([3,0]\phi_u)$	0.126	$([0,0]\sigma_g)([2,0]\delta_g)([2,0]\delta_g)$	0.124
$1\,^2\Delta_g$	$([0,0]\sigma_g)^2([2,0]\delta_g)$	0.173	$([0,0]\sigma_g)([1,0]\pi_u)([3,0]\phi_u)$	0.143
$1\,^2\Sigma_g^+$	$([0,0]\sigma_g)^2([2,0]\sigma_g)$	0.176	$([0,0]\sigma_g)([2,0]\delta_g)^2$	0.168
$1\,^2\Sigma_g^-$	$([0,0]\sigma_g)([1,0]\pi_u)([1,0]\pi_u)$	0.246	$([0,0]\sigma_g)([1,0]\pi_u)([3,0]\pi_u)$	0.111

Table 6. The two leading configurations and their squared norms for the six lowest quartet states of three electrons confined by an oblate-type harmonic oscillator potential with $(\omega_x, \omega_y, \omega_z) = (0.01, 0.01, 0.1)$.

State	Config. 1	Norm 1	Config. 2	Norm 2
$1\,^4\Sigma_g^-$	$([0,0]\sigma_g)([1,0]\pi_u)([1,0]\pi_u)$	0.633	$([0,0]\sigma_g)([1,0]\pi_u)([3,0]\pi_u)$	0.106
$1\,^4\Phi_u$	$([0,0]\sigma_g)([1,0]\pi_u)([2,0]\delta_g)$	0.535	$([0,0]\sigma_g)([1,0]\pi_u)([4,0]\delta_g)$	0.122
$1\,^4\Pi_u$	$([0,0]\sigma_g)([1,0]\pi_u)([2,0]\delta_g)$	0.321	$([0,0]\sigma_g)([1,0]\pi_u)([2,0]\sigma_g)$	0.164
$2\,^4\Pi_u$	$([0,0]\sigma_g)([1,0]\pi_u)([2,0]\sigma_g)$	0.360	$([0,0]\sigma_g)([1,0]\pi_u)([2,0]\delta_g)$	0.194
$1\,^4\Delta_g$	$([1,0]\pi_u)([1,0]\pi_u)([2,0]\delta_g)$	0.222	$([0,0]\sigma_g)([1,0]\pi_u)([3,0]\phi_u)$	0.213
$2\,^4\Delta_g$	$([0,0]\sigma_g)([1,0]\pi_u)([3,0]\pi_u)$	0.161	$([0,0]\sigma_g)([2,0]\delta_g)([2,0]\sigma_g)$	0.139

Table 7. The CI energy (in au) of the six lowest singlet, triplet, and quintet states of four electrons confined by an oblate-type harmonic oscillator potential with $(\omega_x, \omega_y, \omega_z) = (0.01, 0.01, 0.1)$.

Singlet		Triplet		Quintet	
		$1\,^3\Sigma_g^-$	0.513 018		
$1\,^1\Sigma_g^+$	0.513 153				
		$1\,^3\Pi_u$	0.513 417		
$1\,^1\Delta_g$	0.514 024				
				$1\,^5\Delta_g$	0.514 251
		$1\,^3\Phi_u$	0.515 467		
$1\,^1\Gamma_g$	0.517 268				
		$1\,^3\Gamma_g$	0.517 312		
		$1\,^3H_u$	0.519 609		
				$1\,^5\Sigma_g^-$	0.520 449
		$2\,^3\Pi_u$	0.520 959		
$1\,^1\Pi_u$	0.521 764				
$1\,^1\Sigma_g^-$	0.521 900				
$2\,^1\Delta_g$	0.522 075				
				$1\,^5I_g$	0.522 337
				$1\,^5\Pi_u$	0.524 267
				$1\,^5\Phi_u$	0.524 269
				$2\,^5\Pi_u$	0.524 383

electronic state. It has a slightly higher energy than the lowest singlet and triplet states. It is also seen from this table that there is no dipole-allowed excited state within the six lowest singlet and triplet states. The only dipole-allowed states are the $1\,^5\Pi_u$ and $1\,^5\Phi_u$ states in the quintet manifold. They are dipole allowed from the lowest $1\,^5\Delta_g$ state.

It is noted that the energies, 0.010 016 and 0.010 018, calculated for the two transitions $1\,^5\Pi_u$–$1\,^5\Delta_g$ and $1\,^5\Phi_u$–$1\,^5\Delta_g$ agree with the analytical value 0.01 within an absolute error

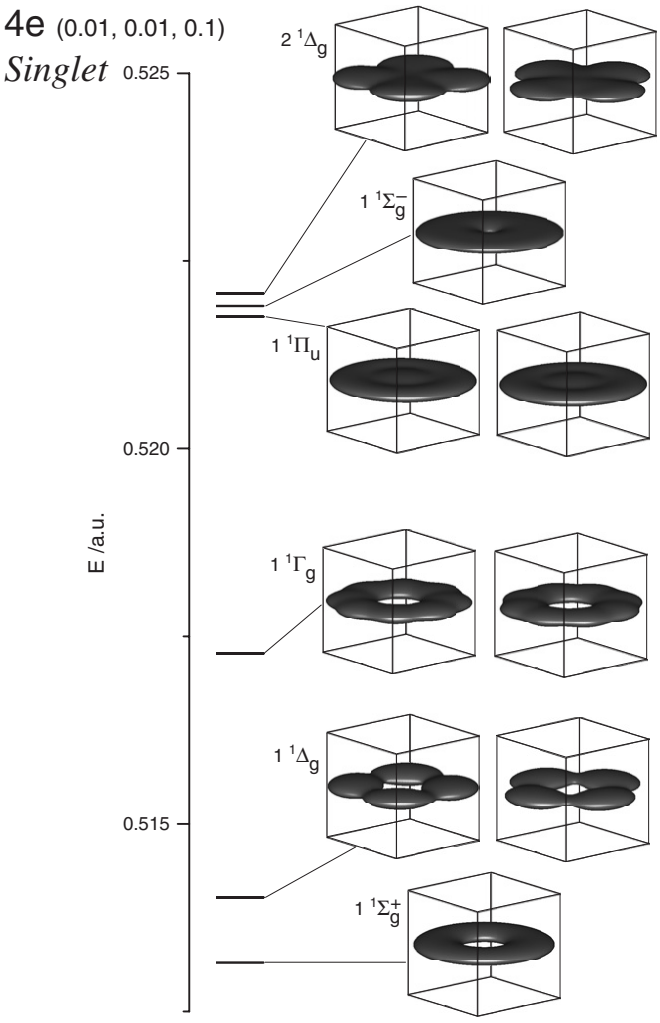

Figure 7. The CI energy and electron density distribution of the six lowest singlet states of four electrons confined by an oblate-type harmonic oscillator potential with $(\omega_x, \omega_y, \omega_z) = (0.01, 0.01, 0.1)$. The density at the surface is 1.0×10^{-4}.

2×10^{-5}. This is significantly larger than the typical error of 1×10^{-6} for the computed transition energies of the two- and three-electron quantum dots. It is shown that this relatively large error for the transition energies of the four-electron quantum dot cannot be made smaller by increasing the number of configurations in the CI wavefunctions, but only by improving the basis set. On adding an m-type function to the reduced c-aniGTO basis set of [1s1p1d1f1g1h1i1j1k1l] the energies for the three states $1\ ^5\Delta_g$, $1\ ^5\Pi_u$, and $1\ ^5\Phi_u$ become 0.514 250, 0.524 254, and 0.524 255, respectively. The corresponding transition energies become 0.010 004 and 0.010 005, with an absolute error less than 5×10^{-6}. This and the previous results of the basis set study in section 2.2 suggest that the basis set needs to be supplemented with higher angular momentum functions as the number of electrons increases.

The two leading configurations of the CI wavefunction and their square norms are listed in tables 8, 9, and 10, respectively, for the six lowest singlet, triplet, and quintet states.

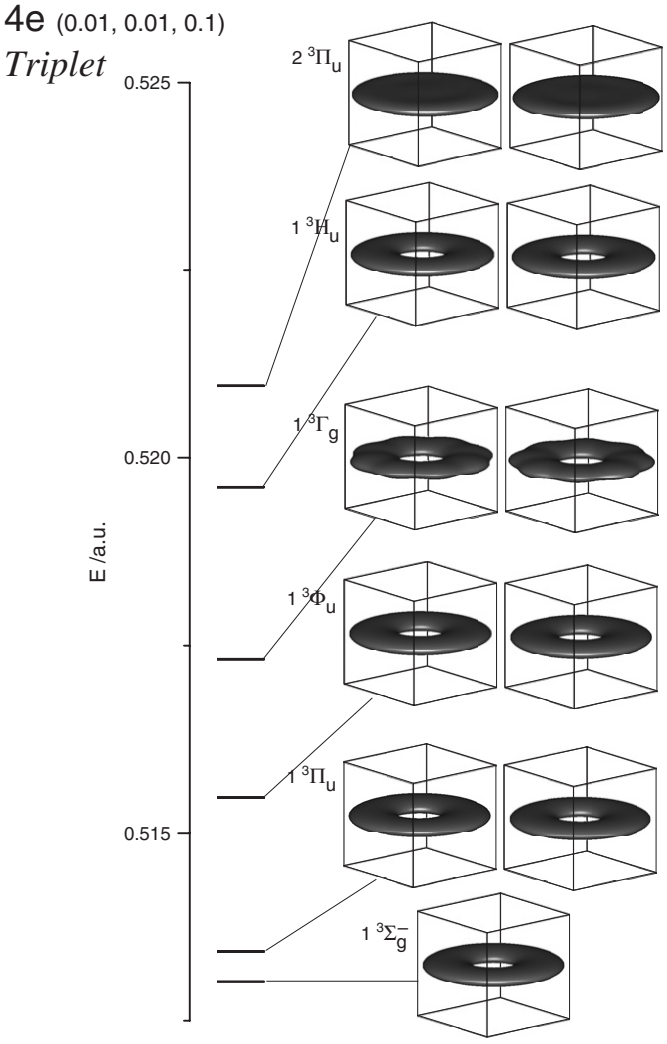

Figure 8. The CI energy and electron density distribution of the six lowest triplet states of four electrons confined by an oblate-type harmonic oscillator potential with $(\omega_x, \omega_y, \omega_z) = (0.01, 0.01, 0.1)$. The density at the surface is 1.0×10^{-4}.

From tables 8 and 9 it is seen that the largest square norm for the leading configuration in the singlet and in the triplet manifold is 0.194 and 0.226, respectively. This indicates that the CI wavefunctions for these low lying singlet and triplet states are dominated by strong configuration mixing. It may be argued that this apparently large configuration mixing is due to the fact that the closed-shell Hartree–Fock orbitals of the two-electron quantum dot are used in the calculation for the four-electron quantum dot. It is noted, however, that the three lowest states in the quintet manifold, $1\ ^5\Delta_g$, $1\ ^5\Pi_u$, and $1\ ^5\Phi_u$, have leading configurations with square norms, 0.568, 0.561, and 0.516, respectively, of a magnitude comparable to that of the leading configuration of the Hartree–Fock ground $1\ ^1\Sigma_g^+$ ground state of the two-electron quantum dot. This result, again, shows that the states with higher spin multiplicity tend to have a smaller configuration mixing than those with lower spin multiplicity as observed already for the two- and three-electron quantum dots.

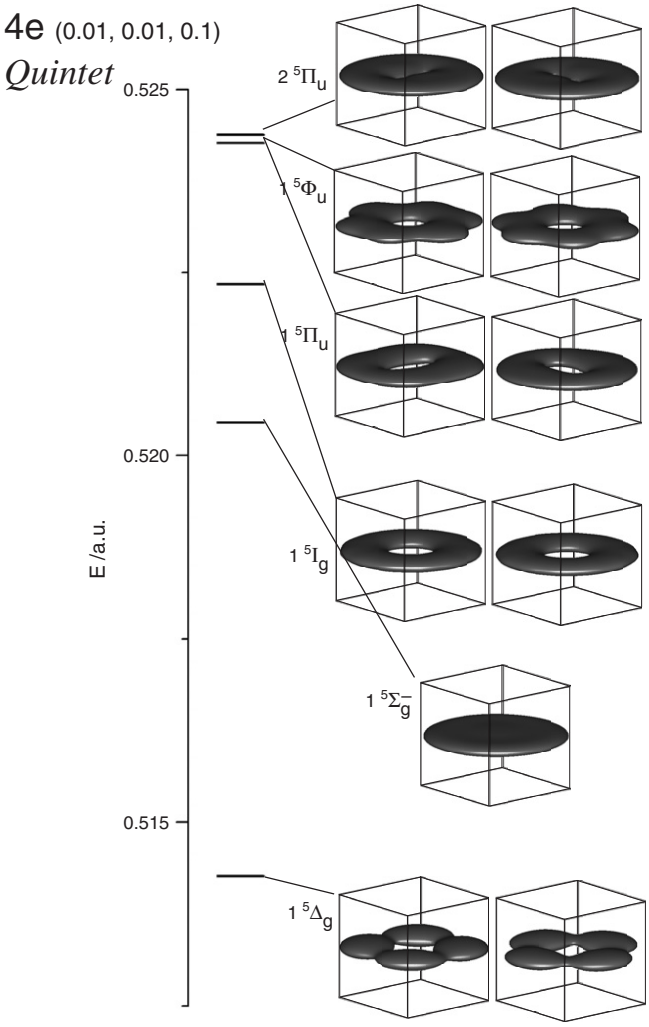

Figure 9. The CI energy and electron density distribution of the six lowest quintet states of four electrons confined by an oblate-type harmonic oscillator potential with $(\omega_x, \omega_y, \omega_z) = (0.01, 0.01, 0.1)$. The density at the surface is 1.0×10^{-4}.

Table 8. The two leading configurations and their squared norms for the six lowest singlet states of four electrons confined by an oblate-type harmonic oscillator potential with $(\omega_x, \omega_y, \omega_z) = (0.01, 0.01, 0.1)$.

State	Config. 1	Norm 1	Config. 2	Norm 2
$1\,^1\Sigma_g^+$	$([1,0]\pi_u)^2([1,0]\pi_u)^2$	0.194	$([0,0]\sigma_g)^2([1,0]\pi_u)^2$	0.125
$1\,^1\Delta_g$	$([0,0]\sigma_g)^2([1,0]\pi_u)^2$	0.194	$([0,0]\sigma_g)([1,0]\pi_u)([1,0]\pi_u)([2,0]\delta_g)$	0.099
$1\,^1\Gamma_g$	$([1,0]\pi_u)([1,0]\pi_u)^2([3,0]\phi_u)$	0.147	$([0,0]\sigma_g)^2([2,0]\delta_g)^2$	0.146
$1\,^1\Pi_u$	$([0,0]\sigma_g)^2([1,0]\pi_u)([2,0]\delta_g)$	0.188	$([0,0]\sigma_g)([1,0]\pi_u)^2([1,0]\pi_u)$	0.095
$1\,^1\Sigma_g^-$	$([0,0]\sigma_g)^2([1,0]\pi_u)([3,0]\pi_u)$	0.135	$([0,0]\sigma_g)([1,0]\pi_u)([1,0]\pi_u)([2,0]\sigma_g)$	0.060
$2\,^1\Delta_g$	$([0,0]\sigma_g)^2([2,0]\delta_g)([2,0]\sigma_g)$	0.150	$([1,0]\pi_u)([1,0]\pi_u)^2([3,0]\pi_u)$	0.078

On inspecting figures 7–9 it is further observed that the low lying energy spectra of the four-electron quantum dot contain states of very high total angular momentum, namely, $1\,^1\Gamma_g$ in

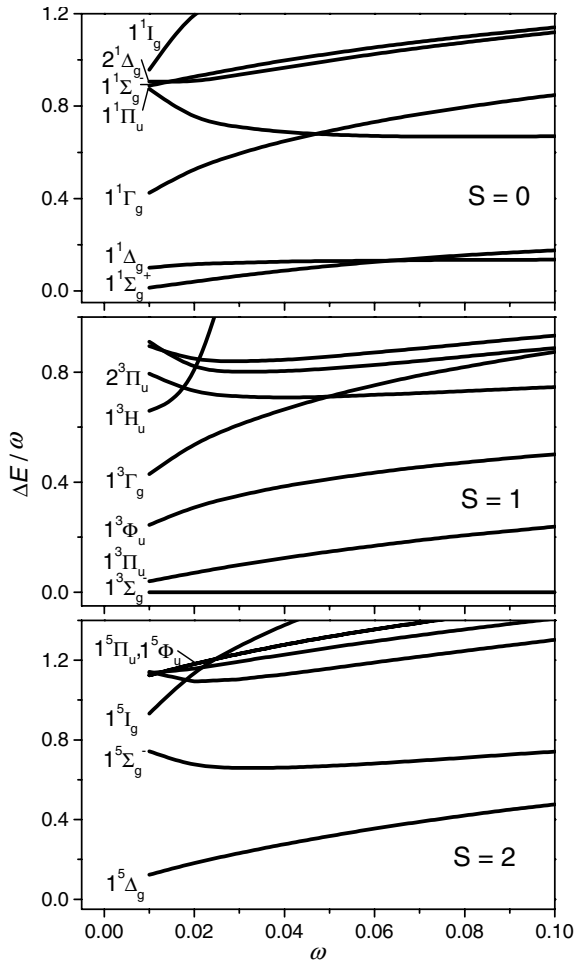

Figure 10. Normalized excitation energy spectra of four electrons confined by an oblate-type harmonic oscillator potential with $(\omega_x, \omega_y, \omega_z) = (\omega, \omega, 10 \times \omega)$ for different ω.

Table 9. The two leading configurations and their squared norms for the six lowest triplet states of four electrons confined by an oblate-type harmonic oscillator potential with $(\omega_x, \omega_y, \omega_z) = (0.01, 0.01, 0.1)$.

State	Config. 1	Norm 1	Config. 2	Norm 2
$1\,^3\Sigma_g^-$	$([0,0]\sigma_g)^2([1,0]\pi_u)([1,0]\pi_u)$	0.226	$([0,0]\sigma_g)([1,0]\pi_u)^2([2,0]\delta_g)$	0.103
$1\,^3\Pi_u$	$([0,0]\sigma_g)([1,0]\pi_u)([1,0]\pi_u)^2$	0.228	$([0,0]\sigma_g)^2([1,0]\pi_u)([2,0]\delta_g)$	0.126
$1\,^3\Phi_u$	$([0,0]\sigma_g)^2([1,0]\pi_u)([2,0]\delta_g)$	0.200	$([1,0]\pi_u)^2([1,0]\pi_u)([2,0]\delta_g)$	0.143
$1\,^3\Gamma_g$	$([0,0]\sigma_g)([1,0]\pi_u)^2([2,0]\delta_g)$	0.119	$([0,0]\sigma_g)^2([1,0]\pi_u)([3,0]\phi_u)$	0.096
$1\,^3H_u$	$([0,0]\sigma_g)([1,0]\pi_u)([2,0]\delta_g)([2,0]\delta_g)$	0.096	$([0,0]\sigma_g)([1,0]\pi_u)([2,0]\delta_g)^2$	0.096
$2\,^3\Pi_u$	$([0,0]\sigma_g)^2([1,0]\pi_u)([2,0]\sigma_g)$	0.158	$([0,0]\sigma_g)([1,0]\pi_u)([1,0]\pi_u)([2,0]\sigma_g)$	0.080

the singlet manifold, $1\,^3\Gamma_g$ and $1\,^3H_u$ in the triplet manifold, and $1\,^5I_g$ in the quintet manifold. This energy level structure of the low lying states of the four-electron quantum dot is very different from that of the conventional few-electron atoms where the low lying energy spectra contain only low angular momentum states, such as S, P, D.

Table 10. The two leading configurations and their squared norms for the six lowest quintet states of four electrons confined by an oblate-type harmonic oscillator potential with $(\omega_x, \omega_y, \omega_z) = (0.01, 0.01, 0.1)$.

State	Config. 1	Norm 1	Config. 2	Norm 2
$1\,^5\Delta_g$	$([0,0]\sigma_g)([1,0]\pi_u)([1,0]\pi_u)([2,0]\delta_g)$	0.568	$([0,0]\sigma_g)([1,0]\pi_u)([2,0]\delta_g)([3,0]\phi_u)$	0.090
$1\,^5\Sigma_g^-$	$([0,0]\sigma_g)([1,0]\pi_u)([1,0]\pi_u)([2,0]\sigma_g)$	0.561	$([0,0]\sigma_g)([1,0]\pi_u)([2,0]\delta_g)([3,0]\pi_u)$	0.095
$1\,^5\mathrm{I}_g$	$([0,0]\sigma_g)([1,0]\pi_u)([2,0]\delta_g)([3,0]\phi_u)$	0.516	$([1,0]\pi_u)([1,0]\pi_u)([2,0]\delta_g)([4,0]\gamma_g)$	0.096
$1\,^5\Pi_u$	$([0,0]\sigma_g)([1,0]\pi_u)([2,0]\delta_g)([2,0]\delta_g)$	0.220	$([0,0]\sigma_g)([1,0]\pi_u)([1,0]\pi_u)([3,0]\pi_u)$	0.115
$1\,^5\Phi_u$	$([0,0]\sigma_g)([1,0]\pi_u)([1,0]\pi_u)([3,0]\phi_u)$	0.334	$([0,0]\sigma_g)([1,0]\pi_u)([2,0]\delta_g)([2,0]\sigma_g)$	0.125
$2\,^5\Pi_u$	$([0,0]\sigma_g)([1,0]\pi_u)([2,0]\delta_g)([2,0]\delta_g)$	0.215	$([0,0]\sigma_g)([1,0]\pi_u)([1,0]\pi_u)([3,0]\pi_u)$	0.130

In order to understand the origin of these low lying high angular momentum states, the *normalized excitation energy*, defined as the excitation energy from the ground $1\,^3\Sigma_g^-$ state divided by the strength of the confinement ω ($=\omega_x = \omega_y$), is plotted in figure 10 for all spin multiplets of $S = 0, 1, 2$. This figure shows that the normalized excitation energy for all high angular momentum states, particularly for the $1\,^1\mathrm{I}_g$, $1\,^3\mathrm{H}_u$, and $1\,^5\mathrm{I}_g$ states, increases very rapidly as ω increases. This indicates that these high angular momentum states are located in the high energy region when ω is large. It shows that the appearance of the high angular momentum states in the low lying energy spectrum is a consequence of the small confinement strength ω. It is noted further that these high angular momentum states cannot be described in terms of a single-electron excitation from the ground state configuration, but only in terms of a multi-electron excitation to *circular modes*. For example, the leading configuration of the $1\,^5\mathrm{I}_g$ state is composed of the four orbitals $([0,0]\sigma_g)$, $([1,0]\pi_u)$, $([2,0]\delta_g)$, and $([3,0]\phi_u)$. Their angular momenta properly added give rise to, among others, the large angular momentum of $L = 6$. Since circular modes correspond to classical circular motions of an electron, the multi-electron excitations in the $1\,^5\mathrm{I}_g$ state correspond to a *coherent circular motion* of the four electrons, that is, all electrons move circularly in the same direction.

The appearance of the high angular momentum states in the low lying energy spectra may be interpreted as follows: the relative importance of the electron repulsion potential for the total energy becomes larger as ω becomes smaller and consequently all electrons begin to move in the same direction in order to keep apart from each other.

4. Summary

The spectrum and the electron density distribution for two, three, and four electrons confined by a strongly anisotropic oblate-type harmonic oscillator potential with small values of ω have been studied for all spin states by using the quantum chemical configuration interaction method employing large Cartesian anisotropic Gaussian basis sets. The convergence of the computed energy spectrum with respect to the size of the basis sets has been examined by checking the degeneracy in the energy spectrum. It is shown that an accuracy of better than 2×10^{-6} has been obtained for the two- and three-electron quantum dots by using basis sets including up to a k-type function, but that in order to achieve similar accuracy for the four-electron quantum dot the basis set has to be supplemented with functions as high as an m-type function. The analysis of the leading configurations in the CI wavefunctions shows that large electron correlation prevails for the low lying states of the systems studied, particularly for the states with a lower spin multiplicity. From the shape of the Hartree–Fock orbital density distributions, two types of characteristic electronic modes are identified, namely, the circular mode and the breathing mode. It is shown that the states having an excitation to the circular

mode are energetically more favourable than the states having an excitation to the breathing mode when the strength of the confinement ω is small.

Acknowledgments

The present study was supported in part by a Grant-in-Aid for Scientific Research (No 16750007) from the Ministry of Education, Science, Sports and Culture. TS thanks the Alexander von Humboldt Foundation for a Research Fellowship from 2000 to 2002, during which period the present study was initiated.

References

[1] Ashoori R C 1996 *Nature* **379** 413–9
[2] Johnson N F 1995 *J. Phys.: Condens. Matter* **7** 965–89
[3] Tarucha S, Austing D G, Honda T, van der Hage R T and Kouwenhoven L P 1996 *Phys. Rev. Lett.* **77** 3613–6
[4] van der Wiel W G, De Franceschi S, Elzerman J M, Fujisawa T, Tarucha S and Kouwenhoven L P 2003 *Rev. Mod. Phys.* **75** 1–22
[5] Antonietti M and Landfester K 2001 *Chem. Phys. Chem.* **2** 207–10
[6] Jaskólski W 1996 *Phys. Rep.* **271** 1–66
[7] Connerade J P, Dolmatov V K and Lakshmi P A 2000 *J. Phys. B: At. Mol. Opt. Phys.* **33** 251–64
[8] Becken W, Schmelcher P and Diakonos F K 1999 *J. Phys. B: At. Mol. Opt. Phys.* **32** 1557–84
[9] Becken W and Schmelcher 2000 *J. Phys. B: At. Mol. Opt. Phys.* **33** 545–68
[10] Fock V 1928 *Z. Phys.* **47** 446–8
[11] Maksym P A and Chakraborty T 1990 *Phys. Rev. Lett.* **65** 108–11
[12] Merkt U, Huser J and Wagner M 1991 *Phys. Rev.* B **43** 7320–3
[13] Taut M 1993 *Phys. Rev.* A **48** 3561–6
[14] Ezaki T, Mori N and Hamaguchi C 1997 *Phys. Rev.* B **56** 6428–31
[15] Sako T and Diercksen G H F 2003 *J. Phys. B: At. Mol. Opt. Phys.* **36** 1433–57
[16] Sako T and Diercksen G H F 2003 *J. Phys.: Condens. Matter* **15** 5487–509
[17] Sun L L, Ma F C and Li S S 2003 *J. Appl. Phys.* **94** 5844–9
[18] Braskén M, Lindberg M, Sundholm D and Olsen J 2000 *Phys. Rev.* B **61** 7652–5
[19] Bielińska-Wąż D, Karwowski J and Diercksen G H F 2001 *J. Phys. B: At. Mol. Opt. Phys.* **34** 1987–2000
[20] Fujito M, Natori A and Yasunaga H 1996 *Phys. Rev.* B **53** 9952–8
[21] Bednarek S, Szafran B and Adamovski J 1999 *Phys. Rev.* B **59** 13036–42
[22] Yannouleas C and Landman U 1999 *Phys. Rev. Lett.* **82** 5325–8
[23] Bryant G W 1987 *Phys. Rev. Lett.* **59** 1140–3
[24] Pfannkuche D, Gudmundsson V and Maksym P 1993 *Phys. Rev.* B **47** 2244–50
[25] Rontani M, Rossi F, Manghi F and Molinari E 1999 *Phys. Rev.* B **59** 10165–75
[26] Cioslowski J and Pernal K 2000 *J. Chem. Phys.* **113** 8434–43
[27] Sako T and Diercksen G H F 2003 *J. Phys. B: At. Mol. Opt. Phys.* **36** 1681–702
[28] Sako T, Cernusak I and Diercksen G H F 2004 *J. Phys. B: At. Mol. Opt. Phys.* **37** 1091–102
[29] Sako T and Diercksen G H F 2003 *J. Phys. B: At. Mol. Opt. Phys.* **36** 3743–59
[30] Sako T, Yamamoto S and Diercksen G H F 2004 *J. Phys. B: At. Mol. Opt. Phys.* **37** 1673–88
[31] Diercksen G H F and Hall G G 1994 *Comput. Phys.* **8** 215–22
[32] Laaksonen L 2003 gOpenMol Program http://www.csc.fi/gopenmol
[33] Corni S, Braskén M, Lindberg M, Olsen J and Sundholm D 2003 *Phys. Rev.* B **67** 085314
[34] Sako T, Aoki D, Yamanouchi K and Iachello F 2000 *J. Chem. Phys.* **113** 6063–9
[35] Kohn W 1961 *Phys. Rev.* **123** 1242–4
[36] Brey L, Johnson N F and Halperin B I 1989 *Phys. Rev.* B **40** 10647–9
[37] Peeters F M 1990 *Phys. Rev.* B **42** 1486–7
[38] Li Q P, Karraï K, Yip S K, Das S S and Drew H D 1991 *Phys. Rev.* B **42** 1486–7
[39] Szafran B, Adamowski J and Bednarek S 2000 *Physica* E **5** 185–95